Ultra-wideband Time Difference of Arrival Indoor Localization: From Sensor Placement to System Evaluation

Wenda Zhao[1†], Abhishek Goudar[1†], Mingliang Tang[1,3†], and Angela P. Schoellig[1,2]
[1] University of Toronto Institute for Aerospace Studies,
Vector Institute for Artificial Intelligence, Canada
[2]Technische Universität München,
Munich Institute for Robotics and Machine Intelligence, Germany
[3]University of California Berkeley, United States

Wireless indoor localization has attracted significant research interest due to its high accuracy, low cost, lightweight design, and low power consumption. Specifically, ultra-wideband (UWB) time difference of arrival (TDOA)-based localization has emerged as a scalable positioning solution for mobile robots, consumer electronics, and wearable devices, featuring good accuracy and reliability. While UWB TDOA-based localization systems rely on the deployment of UWB radio sensors as positioning landmarks, existing works often assume these placements are predetermined or study the sensor placement problem alone without evaluating it in practical scenarios. In this article, we bridge this gap by approaching the UWB TDOA localization from a system-level perspective, integrating sensor placement as a key component and conducting practical evaluation in real-world scenarios. Through extensive real-world experiments, we demonstrate the accuracy and robustness of our localization system, comparing its performance to the theoretical lower bounds. Using a challenging multi-room environment as a case study, we illustrate the full system construction process, from sensor placement optimization to real-world deployment. Our evaluation, comprising a cumulative total of 39 minutes of real-world experiments involving up to five agents and covering 2608 meters across four distinct scenarios, provides valuable insights and guidelines for constructing UWB TDOA localization systems.

***Index Terms*—Localization, Sensor Fusion, Hardware-Software Integration in Robotics**

I. Introduction

Indoor localization technology is rapidly advancing, offering a promising future where accurate positioning enables a broad spectrum of applications, including robotics, virtual/augmented reality (VR/AR), and seamless navigation with location-based services. Precise localization and ubiquitous communication have become essential expectations for the sixth generation (6G) wireless systems [1]. A conceptual diagram demonstrating the indoor positioning service in a shopping mall is shown in Figure 1. For indoor robotics applications, visual-inertial odometry (VIO) and visual simultaneous localization and mapping (SLAM) are commonly employed techniques to achieve precise 6 degrees-of-freedom localization, with cameras providing the main source of information. However, visual localization algorithms might face challenges under dynamic lighting conditions and partial or temporary occlusion of the cameras. More importantly, capturing raw images of the surrounding environment will pose challenges for security and privacy [2].

Compact and computationally-constrained indoor robots and smart devices have led researchers to pursue localization methods leveraging low-power and lightweight sensors. Ultra-wideband (UWB) radio technology has been shown to provide potential high-accuracy time of arrival (TOA) measurements with low power consumption compared to commonly used sensors such as camera, radar, and light detection and ranging (LiDAR) in the field of robotics. UWB chips have been integrated into the latest generations of consumer electronics including smartphones and smartwatches to support low-latency spatially-aware interactions [3].

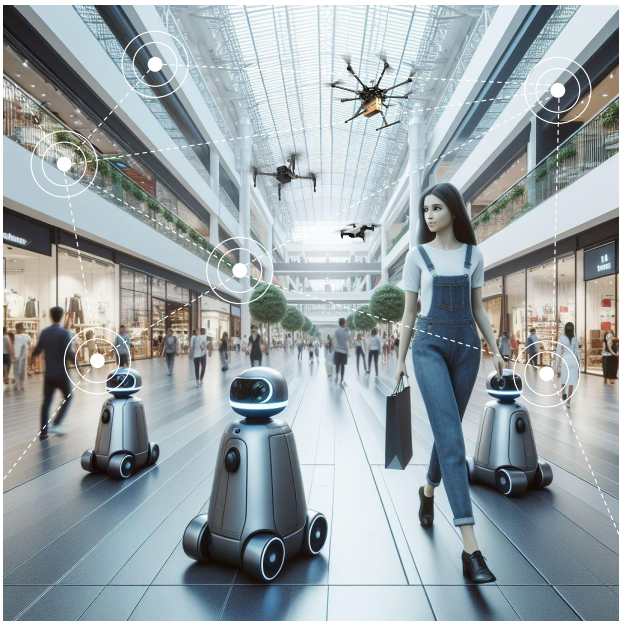

Fig. 1. A conceptual diagram demonstrating the deployment of an indoor localization system in a shopping mall. The image illustrates heterogeneous agents, including ground robots and flying robots, leveraging the indoor positioning system to navigate seamlessly alongside customers while providing various services, such as item delivery or cleaning service. (This conceptual image is created from an image we generated using DALL·E 3 text-to-image models developed by Open AI.)

Manuscript received XX; revised XX, 2024. † These authors contribute equally to this work. Corresponding author: W. Zhao (email: wenda.zhao@robotics.utias.utoronto.ca).

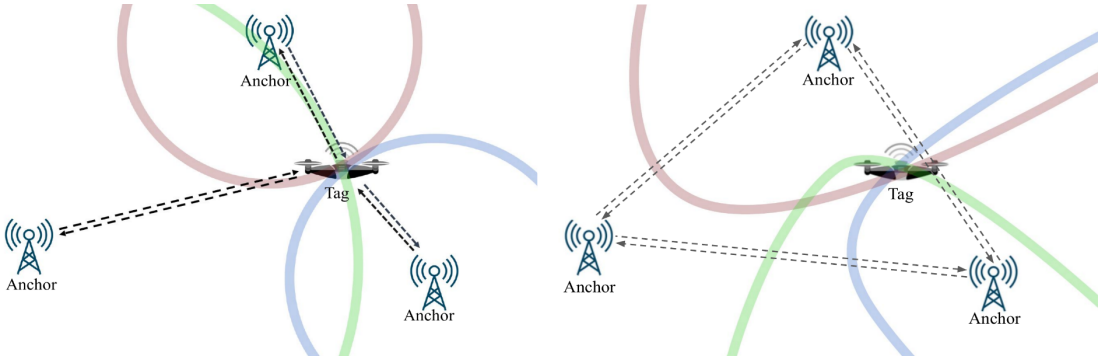

Fig. 2. Conceptual diagrams for UWB TWR (left) and TDOA (right) localization system. In TWR, the UWB tag actively communicates with UWB anchors for localization. In TDOA, the UWB tag listens to the communications between anchors passively for positioning.

Similar to the Global Positioning System (GPS) [4], a UWB-based positioning system requires UWB radios (also called anchors) to be pre-installed in the environment as a constellation with known positions, which in turn serve as landmarks for positioning. In robotics, the two main ranging schemes used for UWB localization are *(i)* two-way ranging (TWR) and *(ii)* time difference of arrival (TDOA) (see Figure 2). In TWR, the UWB module mounted on the robot (also called the tag) communicates with an anchor and acquires range measurements through two-way communication. In TDOA, UWB tags compute the difference between the arrival times of the radio packets from two anchors as TDOA measurements. Compared with TWR, TDOA does not require active two-way communication between an anchor and a tag, thus enabling localization of a large number of devices. This scalability is crucial for scenarios that require localizing numerous agents simultaneously, such as providing positioning service for customers in large shopping malls and coordinating hundreds of drones for indoor drone shows. Therefore, we focus on developing UWB TDOA-based localization systems to facilitate the coordination of a large number of agents.

Considerable attention has been devoted to mitigating non-line-of-sight (NLOS) and multi-path radio propagation to enhance UWB-aided localization performance. However, these studies often assume the placement of UWB anchors is predetermined and overlook its critical impact on the localization performance. Existing sensor placement studies [5] primarily focus on finding a theoretically optimal sensor placement solution under restrictive assumptions, which often encounter challenges when applied to real-world cluttered scenarios. In our previous work [6], we proposed a more realistic optimal sensor placement algorithm that considers obstacles and multi-room scenarios. However, we only conducted simulation and static experiments in a lab setup without evaluating the algorithm in practical scenarios. In this article, we fill this gap by approaching the UWB TDOA localization from a system-level perspective, integrating sensor placement as a key component and conducting practical evaluation in real-world environments. Using pedestrian tracking problem as an example, we fuse UWB TDOA measurements with a low-cost inertial measurement unit (IMU) sensor to achieve 6 degrees-of-freedom pose estimates. We employ an error-state Kalman filter (ESKF), favored for its widespread use and effectiveness in practical applications, and compare our results against the theoretical lower bound. Using a challenging multi-room environment as a case study, we demonstrate the entire process of setting up a UWB TDOA localization system, from optimizing UWB anchor placement to deploying and testing the system in a real-world environment. To the best of our knowledge, this comprehensive evaluation, presenting a UWB TDOA-based localization system from a system-level perspective, has not been shown in the literature. A video summarizing our experiment process is available at http://tiny.cc/uwb_tdoa_ram24. Our main contributions can be summarized as follows:

- We present a system-level approach to UWB TDOA localization, incorporating sensor placement as a fundamental component.
- We demonstrate the accuracy and robustness of the localization system through extensive real-world experiments and compare its performance to theoretical lower bounds.
- We present the entire process of setting up a UWB TDOA localization system in a real-world multi-room environment, from sensor placement optimization to system deployment and evaluation against the theoretical analysis.
- We will release the datasets collected during our experiments upon the acceptance of this work to benefit the research community.

II. Related Work

As UWB measurements, like any other radio frequency (RF) signals, are often affected by obstacle-induced NLOS and multi-path radio propagation, multiple approaches have been proposed to improve localization accuracy under measurement corruption. M-estimators [7] are commonly used as versatile tools to mitigate the influence of measurement outliers by employing robust cost functions to downweight the impact of large measurement residuals. Researchers have also explored novel models to represent UWB measurement residuals including both parametric [8] and non-parametric models, such as neural networks [9], Gaussian processes [10], and Gaussian mixture models [11], aiming to enhance localization performance. Furthermore, continuous-time estimation

techniques [12], [13] have garnered attention and have been investigated for their applicability in asynchronous UWB-aided localization systems.

The anchor-tag geometry is widely recognized as a significant contributing factor to the performance of TDOA-based localization. Consequently, ensuring an optimized design for the placement of UWB anchors is crucial to guarantee reliable and accurate positioning performance. The sensor placement problem has most notably been studied by the GPS community. Geometric dilution of precision (GDOP) is a classical performance metric widely used to evaluate the quality of a GPS satellite configuration [14]. Cramér-Rao lower bound (CRLB) [15] is a more general performance metric for sensor placement, which considers statistical properties of sensor measurements to evaluate estimation performance. In our previous work [6], we extended the optimal sensor placement analysis to balance the effects of anchor-tag geometry and NLOS measurement biases in cluttered indoor environments. However, our experimental validation process was limited to static experiments conducted in a laboratory setup, using multilateration as the position estimator.

In this article, we present a UWB TDOA localization system approached from a system-level perspective, integrating sensor placement as a crucial component and evaluating it through practical experiments in real-world scenarios. To achieve 6 degrees-of-freedom poses while maintaining a low-power and lightweight design, we fuse UWB TDOA measurements with a low-cost IMU sensor through an error-state Kalman filter (ESKF) [16]. The integration and evaluation of this system in real-world settings demonstrate the impact of sensor placement within a complete localization framework. Through a comprehensive case study in a challenging multi-room environment, we illustrate the entire process of system construction, from sensor placement optimization to real-world deployment. We evaluate the localization performance by comparing it to the corresponding theoretical analysis, which provides valuable insights and guidelines for developing UWB TDOA localization systems.

III. UWB TDOA Localization System

In the following section, we provide an overview of our UWB TDOA localization system. We first introduce the sensor placement optimization and the UWB TDOA-IMU localization algorithm. Then, we present the hardware and software architecture of our UWB TDOA localization system as well as the details of system deployment. The overall system architecture is shown in Figure 3.

A. Preliminaries and Notation

A general UWB TDOA-based localization system consists of a set of m UWB anchors, divided into anchor pairs $\Gamma = \{(1,2),(2,3),\cdots,(m-1,m)\}$ that are pre-installed in an indoor space $\mathcal{P} \in \mathbb{R}^3$. To facilitate our analysis, we define a vector $\boldsymbol{\alpha} = \left[\boldsymbol{a}_1^T, \boldsymbol{a}_2^T, \cdots, \boldsymbol{a}_m^T\right]^T \in \mathbb{R}^{3\cdot m}$ to denote the anchor placement. Five handheld devices are designed for localization purposes, each equipped with one IMU and one UWB tag. We refer to the absolute coordinate frame created by the UWB anchors as the inertial frame $\mathcal{F}_{\mathcal{I}}$ and denote the handheld device body frame as $\mathcal{F}_{\mathcal{B}}$.

B. Sensor Placement Optimization

Sensor placement optimization is often conducted through the lens of statistical parameter estimation, which optimizes the performance bounds for estimating the parameters of interest with a given model. Considering the UWB TDOA localization system in particular, we analyze the lower bound on the position estimate based on the UWB anchor placement and the TDOA measurement model. This analysis provides insights into the fundamental limitations of the system's localization accuracy. In our previous work [6], we leverage the mean-squared error (MSE) metric to evaluate the UWB TDOA localization performance for a region of interest in cluttered environments. The estimated tag position $\hat{\mathbf{p}}$ is characterized by its bias $\text{Bias}(\hat{\mathbf{p}})$ and covariance matrix $\text{Cov}(\hat{\mathbf{p}})$. The MSE of an estimate $\hat{\mathbf{p}}$ of the true value $\mathbf{p}$ can be decomposed as

$$\text{MSE}(\hat{\mathbf{p}}) = \mathbb{E}\{\|\hat{\mathbf{p}} - \mathbf{p}\|^2\} = \text{Tr}\left(\text{Cov}(\hat{\mathbf{p}})\right) + \|\text{Bias}(\hat{\mathbf{p}})\|^2, \quad (1)$$

where $\text{Tr}(\cdot)$ is the trace operator and $\|\cdot\|$ is the ℓ_2 norm. Based on the uniform Cramér-Rao bound [17] and linear approximation, we can compute the lower bound of the $\text{MSE}(\hat{\mathbf{p}})$, denoted as $M(\mathbf{p}, \boldsymbol{\alpha})$, with respect to a given anchor placement $\boldsymbol{\alpha}$. For a region or a trajectory of interest, we evaluate the MSE metric at N sample points $\mathbf{p}_i \in \Phi, i = 1 \cdots N$, and compute the average root-mean-squared error (RMSE)

$$\mathcal{M}(\boldsymbol{\alpha}) = \frac{1}{N}\sum_{i=1}^{N}\sqrt{M(\mathbf{p}_i, \boldsymbol{\alpha})} \quad (2)$$

as the performance metric of the sensor placement $\boldsymbol{\alpha}$.

Optimal anchor placement is essential for ensuring reliable localization performance in UWB TDOA localization systems, particularly in cluttered and geometrically challenging environments. Therefore, it is important to optimize the anchor positions for regions or trajectories of interest during system design. We define a set $\mathcal{A}$ containing all possible anchor configurations with $\boldsymbol{\alpha} \in \mathcal{A}$ and use a block coordinate-wise minimization (BCM) algorithm to find the optimal placement of UWB anchors $\boldsymbol{\alpha}^\star$ that minimizes $\mathcal{M}(\boldsymbol{\alpha})$:

$$\boldsymbol{\alpha}^\star = \underset{\boldsymbol{\alpha}\in\mathcal{A}}{\text{argmin}}\, \mathcal{M}(\boldsymbol{\alpha}). \quad (3)$$

Readers are encouraged to refer to [6] for a comprehensive explanation of the aforementioned optimal sensor placement algorithm.

C. UWB TDOA-Inertial Navigation System

To achieve 6 degrees-of-freedom pose estimation, we fuse UWB TDOA measurements with an IMU sensor, leading to a UWB TDOA-inertial navigation system. We follow the parameterization from [18] and describe the system with a 16-dimensional state vector:

$$\mathbf{x}(t) = (\mathbf{p}(t), \mathbf{v}(t), \mathbf{q}_{\mathcal{IB}}(t), \mathbf{b}_a(t), \mathbf{b}_\omega(t)), \quad (4)$$

where $\{\mathbf{p}(t), \mathbf{v}(t), \mathbf{q}_{\mathcal{IB}}(t)\}$ denote the position, linear velocity, and orientation of the IMU body frame with respect to the

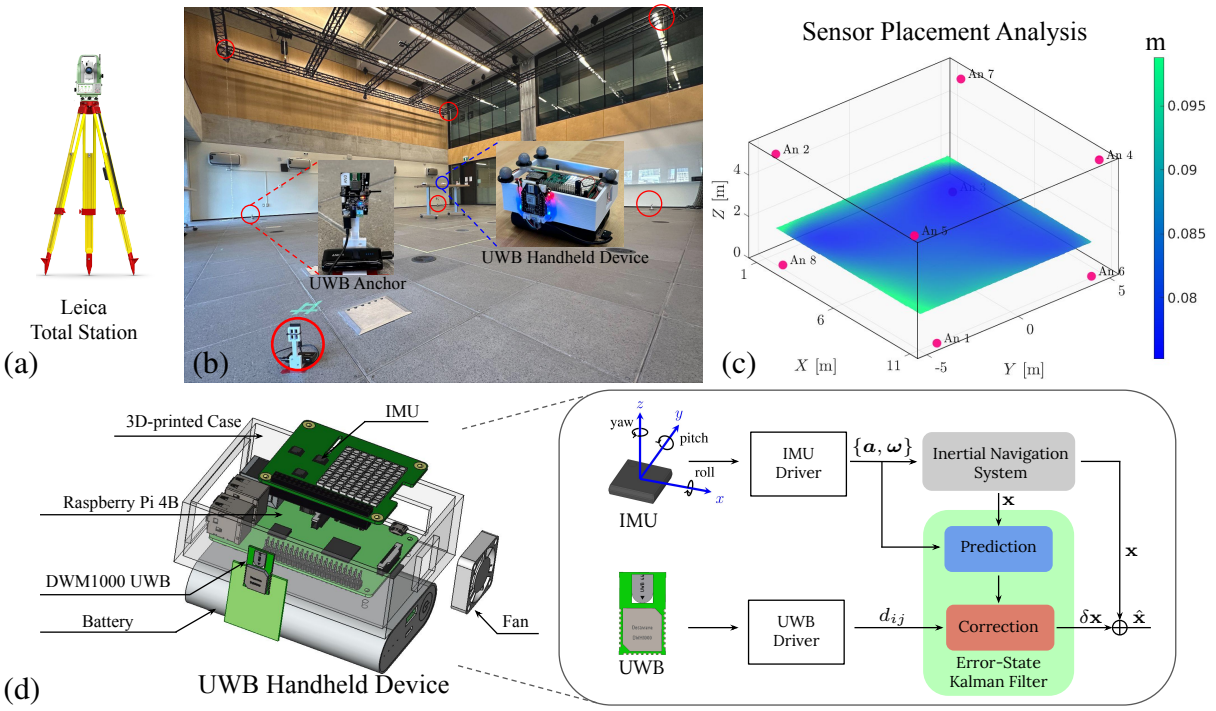

Fig. 3. The system diagram provides a comprehensive overview of each component in our UWB TDOA localization system. The experimental setup of the multi-agent pedestrian localization is shown in (b). UWB anchors, enclosed by red circles, are installed in the space with positions surveyed by a Leica total station (a). The heatmap in (c) illustrates the localization performance of the anchor constellation shown in (b), calculated at a height of 1.5 meters using sensor placement analysis. Lower root-mean-squared error (RMSE) is indicated as darker color. The hardware components of our UWB handheld device along with the onboard ESKF localization algorithm are shown in (d).

inertial frame. A unit quaternion parameterization is used for representing orientations. Accelerometer and gyroscope biases are denoted by $\mathbf{b}_a(t)$ and $\mathbf{b}_\omega(t)$. The spatial offset, also called lever-arm, between the IMU and UWB tag is denoted by $\boldsymbol{l}_{ub}$.

The measured angular rate by a gyroscope $\boldsymbol{\omega}_m = (\omega_x, \omega_y, \omega_z)$ is related to the true angular rate $\boldsymbol{\omega}_t$ as: $\boldsymbol{\omega}_m = \boldsymbol{\omega}_t + \mathbf{b}_\omega + \mathbf{n}_\omega$, where $\mathbf{b}_\omega$ is the time-varying bias and $\mathbf{n}_{b\omega}$ is a zero-mean additive white Gaussian noise (AWGN) process with covariance $\mathbf{Q}_\omega$, i.e. $\mathbf{n}_\omega \sim \mathcal{N}(\mathbf{0}, \mathbf{Q}_\omega)$. The bias is modelled as driven by another AWGN process $\mathbf{n}_{b\omega} \sim \mathcal{N}(\mathbf{0}, \mathbf{Q}_{b\omega})$: $\dot{\mathbf{b}}_\omega = \mathbf{n}_{b\omega}$. A similar model is used for the accelerometer.

To facilitate the localization of multiple heterogeneous agents, the motion model used in this work is a 3D kinematic motion model with IMU measurements as inputs [18]. This is generally referred to as an inertial navigation system (INS). The relevant equations and a detailed description of the motion model can be found in [18]. The UWB TDOA measurements complement the motion dynamics by providing drift-free difference-of-distance measurements between UWB anchor pairs and the UWB tag. The measurement model for an anchor pair $\{\boldsymbol{a}_i, \boldsymbol{a}_j\}$ is described as follows:

$$d_{ij,t} = \|\mathbf{C}_{\mathcal{IB}}(t)\boldsymbol{l}_{ub} + \mathbf{p}(t) - \boldsymbol{a}_j\| - \|\mathbf{C}_{\mathcal{IB}}(t)\boldsymbol{l}_{ub} + \mathbf{p}(t) - \boldsymbol{a}_i\| + \eta_{ij}(t), \tag{5}$$

where $\mathbf{C}_{\mathcal{IB}}(t) := \mathbf{C}\{\mathbf{q}_{\mathcal{IB}}(t)\}$ represents the rotation matrix from the body frame to the inertial frame. The UWB measurement noise, denoted as $\eta_{ij}(t)$, is modeled to follow a zero-mean Gaussian distribution $\eta_{ij} \sim \mathcal{N}(0, \sigma_{ij}^2)$ and is assumed to be common to all TDOA measurements.

To estimate the system state, we select the ESKF [16] algorithm for its proven effectiveness and widespread use in practical applications. In this formulation, inertial dead reckoning is used to propagate the state (4) forward in time using a 3D kinematic motion model with the IMU measurements as inputs. The uncertainty associated with dead reckoning is estimated in the prediction step. In the correction step, the error in the predicted state and the corresponding uncertainty are estimated using the UWB measurements. The error state corresponding to the state (4) is

$$\delta\mathbf{x} = (\delta\mathbf{p}, \delta\mathbf{v}, \delta\boldsymbol{\theta}, \delta\mathbf{b}_a, \delta\mathbf{b}_\omega), \tag{6}$$

where $\delta\mathbf{p}$ and $\delta\mathbf{v}$ represent the errors in IMU position and linear velocity, respectively. Errors in the accelerometer and gyroscope biases are represented by $\delta\mathbf{b}_a$ and $\delta\mathbf{b}_\omega$, respectively. The local angular error $\delta\boldsymbol{\theta}$ is related to small differential rotations $\delta\mathbf{q}$ by: $\delta\mathbf{q} = \left(1, \frac{1}{2}\delta\boldsymbol{\theta}\right)$, $|\delta\boldsymbol{\theta}| \ll 1$.

The correction step estimates the error between the dead reckoned state and the state consistent with UWB TDOA measurements. The estimated error (6) is then composed with the state to compensate for the accumulated drift: $\hat{\mathbf{x}} = \mathbf{x} \oplus \delta\mathbf{x}$, where $\oplus$ is a generic composition operator which represents *(i)* quaternion multiplication for the orientation error, $\mathbf{q} = \mathbf{q} \otimes \delta\mathbf{q}$, and *(ii)* the addition operation for the remaining states, $\mathbf{p} = \mathbf{p} + \delta\mathbf{p}$. We refer the reader to [19] for a description of the prediction and correction step of the ESKF.

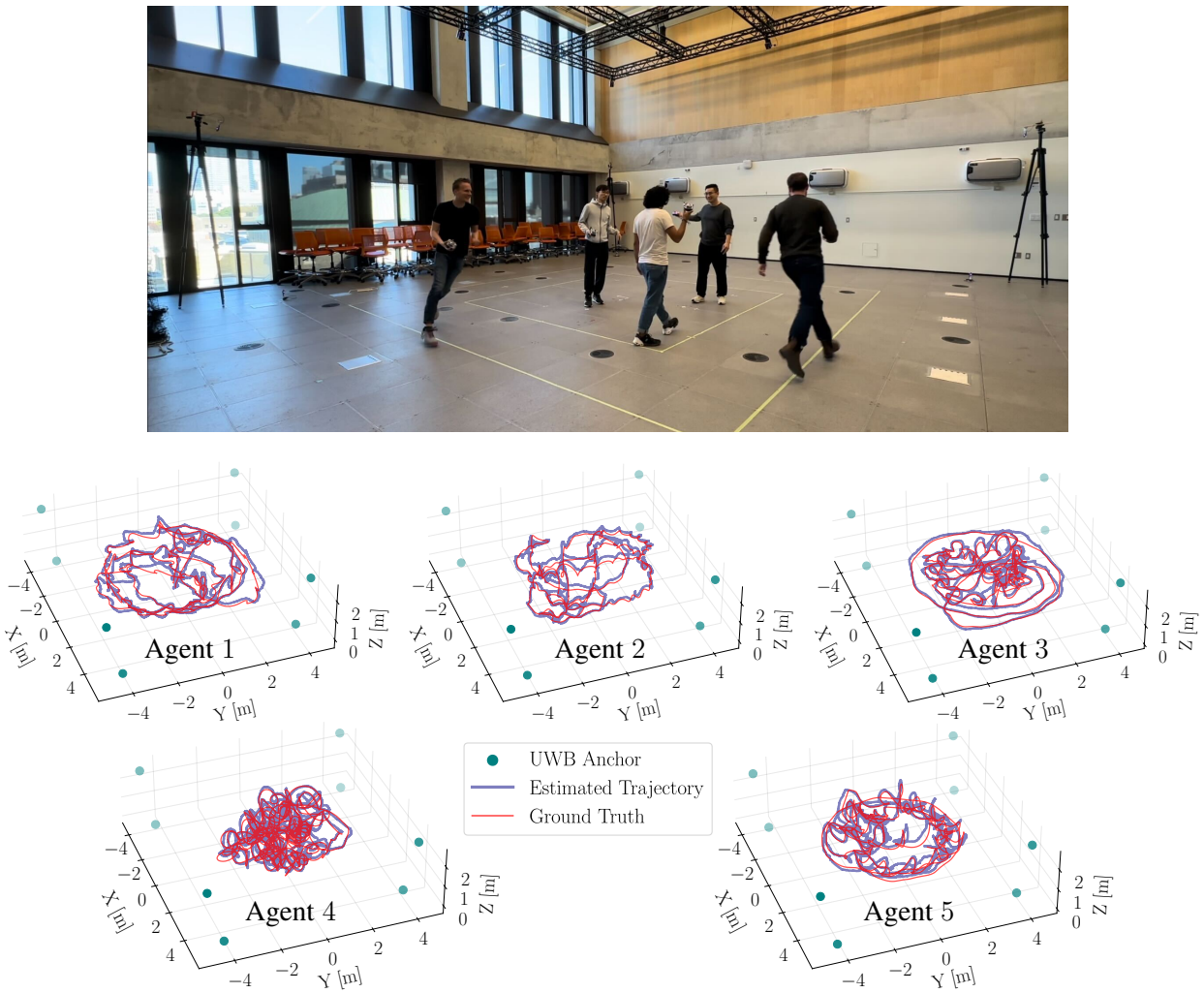

Fig. 4. The multi-agent pedestrian localization experiment with five agents in constellation 1 is shown in the photo above. The estimated together with the ground truth trajectories of each agent during the experiments are shown in the bottom plots. Readers are encouraged to view our supplementary video (http://tiny.cc/uwb_tdoa_ram24) to gain a better insight into our experimental process and evaluate the robustness of the localization performance.

D. System Architecture and Deployment Details

To evaluate localization performance, we assembled five UWB handheld devices, as shown in Figure 3d, specifically designed for multi-agent localization purposes. We leveraged the Loco Positioning System (LPS) from Bitcraze, which employs low-cost DWM1000 UWB radios, to construct our UWB TDOA localization system. To maintain cost-effectiveness, each handheld device is equipped with an inexpensive STMicro LSM9DS1 IMU and a DWM1000 UWB tag. The onboard computer for each device is a Raspberry Pi 4 Model B with 8GB RAM, paired with a power bank serving as the power supply. These elements are assembled within a 3D-printed case for portability. The total cost for a baseline system, including eight LPS UWB anchors from Bitcraze and one handheld device, falls below 2000 USD using commercially available components, which can be further reduced by using raw sensor modules.

To enhance the portability of the localization system, all hardware components are configured as plug-and-play, including both the anchors and the handheld devices. The onboard computer on each handheld device runs an Ubuntu 20.04 LTS operating system, using Robot Operating System (ROS) Noetic as the middleware. The ESKF localization algorithm is implemented in C++ and runs at a frequency of 420 Hz, consuming approximately 35% of a single CPU core and 0.4% of the onboard computer's RAM.

During the system deployment, we use a millimeter-accurate Leica total station (see Figure 3a) to establish the inertial frame and survey each anchor's position in this frame. Utilizing the "Orientate to line" method in the Leica Captivate surveying field software, we surveyed two points to define the "East axis", with the first serving as the origin and the second along the x-axis of the inertial frame we aim to define. After establishing the inertial frame, we conducted a survey of the pre-installed UWB anchors, measuring their 3D positions within this inertial frame with millimeter-level accuracy. Our UWB localization system provides drift-free positioning relative to the established inertial frame.

IV. Experiments

To fully demonstrate the localization performance of our UWB TDOA localization system, we conducted extensive experiments in a variety of real-world environments. We first demonstrate the multi-agent pedestrian localization performance and compare the localization accuracy resulting from two different anchor placements. Then we showcase the system's ability to provide reliable positioning services under sensor occlusion. Furthermore, we demonstrate how sensor placement analysis effectively evaluates the degradation in positioning performance caused by the challenging anchor-tag geometry in a staircase scenario. Finally, using a challenging multi-room environment composed of a cafeteria and a narrow hallway as a case study, we illustrate the entire construction process of our UWB TDOA localization system, from sensor placement optimization to real-world deployment, and evaluate the localization performance compared to the theoretical lower bounds. A video summarizing our experiment process is available at http://tiny.cc/uwb_tdoa_ram24.

A. Multi-agent Pedestrian Localization

We first demonstrate the accuracy and robustness of our UWB TDOA positioning system in multi-agent pedestrian localization through comprehensive real-world experiments. We used eight DWM1000 UWB radios as anchors to set up the UWB TDOA localization system. The anchors were configured to be in centralized TDOA mode and communicated in a round-robin network topology with $\Gamma = \{(8,1),(1,2),\cdots,(7,8)\}$. A detailed explanation of centralized and decentralized TDOA modes using Bitcraze's UWB anchors can be found in [20]. Given that the experimental space is an open, two-story indoor flight arena, we put the anchors at the corners of the space to maximize the coverage of the positioning area (see Figure 3b). The standard deviation of the UWB TDOA measurement noise is set to be $\sigma_{ij} = 0.1$ m, which is the default DWM1000 UWB radio precision. We applied a chi-squared test in the ESKF algorithm as the outlier rejection mechanism with the Mahalanobis distance parameter set to 5. We treat the millimeter-level positioning provided by a Vicon motion capture system as the ground truth. Although the UWB TDOA localization system can provide positioning services to an unlimited number of agents, we demonstrate the multi-agent pedestrian localization performance using five identical handheld devices in our experiments.

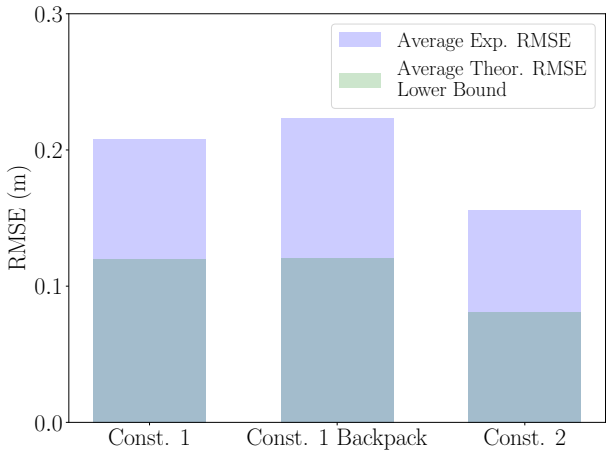

Fig. 5. Comparison of the average experimental root-mean-square error (RMSE) for multi-agent pedestrian localization in Const. 1 and 2, along with localization under occlusion in Const. 1 (Const. 1 Backpack), shown as blue bars, against the theoretical RMSE lower bounds represented by green bars.

We conducted similar experiments using two different anchor constellations. In the first constellation, four anchors were placed on the tripods at a height of 2.65 meters, leading to a narrower separation in the z-axis. Over three experiment trials, five participants each carried a handheld device and navigated within the convex hull of the anchor constellation. While walking and running freely, the students waved the handheld devices, engaging in a variety of movements within the space. We demonstrate one trial of our experiments together with a comparison of the estimated and the ground truth trajectories for each agent in Figure 4. We invite readers to view our supplementary video (http://tiny.cc/uwb_tdoa_ram24) to gain a better insight into our experimental process and evaluate the robustness of the localization performance. Across the three experimental trials, our localization system demonstrated consistent pedestrian localization performance for the five agents, achieving an average RMSE of 21 centimeters with a small standard deviation of 1.56 centimeters. In the second anchor constellation, we mounted the four anchors on the room's ceiling frame, increasing the z-axis separation to 5.5 meters. Similarly, three students carried the handheld devices and conducted three trials of experiments by walking around the same room. With identical parameters applied in the ESKF algorithm, the average RMSE for the three experiments in the second constellation is 16 centimeters with a similar standard deviation of 1.63 centimeters.

Through these comparative experiments, we observe that changing the sensor placement alone leads to a notable impact on the localization performance, which highlights the importance of UWB anchor placement. We calculate the theoretical lower bounds of localization RMSE in the aforementioned two anchor constellations using sensor placement analysis. The average theoretical RMSE lower bounds in the first and second anchor constellations are 12 centimeters and 8 centimeters, respectively. We summarize the average experimental RMSE values for multi-agent pedestrian localization and the theoretical RMSE lower bounds in Figure 5 for comparison. The experimental results agree with the theoretical analysis that sensor placements with lower theoretical RMSE bounds generally yield better localization performance.

B. Localization under Sensor Occlusion

One distinctive feature of UWB-Inertial localization is that the sensor set can be partially or completely occluded thanks to the obstacle-penetrating ability of UWB measurements. To demonstrate this feature, we put one UWB handheld device into a backpack (see Figure 6) and conducted three trials of experiments in the aforementioned first anchor constellation. Since the device was completely occluded by the backpack throughout the experiments, we created a motion capture

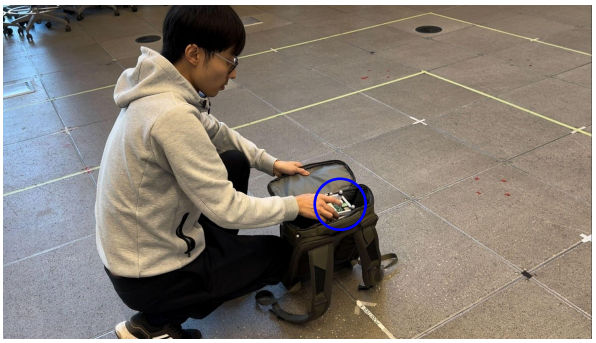

Fig. 6. The UWB handheld device, highlighted by a blue circle, was put into a backpack to demonstrate the localization performance under sensor occlusion.

tracking object for the backpack to record the ground truth position data approximately. As before, we summarize the average localization RMSE over three experimental trials together with the theoretical lower bound value in Figure 5. Readers are encouraged to view our supplementary video to gain an intuitive understanding of this experimental process.

The average RMSE from the three experiments is 22 centimeters, which closely matches the performance of multi-agent pedestrian localization (21 centimeters) within the same constellation. Although the fabric backpack did not pose a severe NLOS challenge for UWB measurements, conventional localization algorithms relying on cameras or LiDARs are unsuitable for this application. This result demonstrates that the UWB-inertial localization system has the potential to provide reliable positioning performance even under complete sensor occlusion.

C. Localization in a Staircase Environment

Realistic working conditions, such as building monitoring or multi-room scenarios, often pose geometric challenges that can impact UWB TDOA localization performance. The presence of challenging anchor-tag geometry in such environments often leads to degradation in localization accuracy. Consequently, evaluating localization performance through sensor placement analysis is crucial to avoid areas with poor positioning accuracy. To showcase this ability, we conducted experiments in a geometrically challenging staircase environment. We illustrate how sensor placement analysis effectively captures the degradation of localization accuracy induced by the difficult anchor-tag geometry in staircase positioning scenarios.

The staircase scenario and our experimental setup are shown in Figures 7a and b. Similar to the experiments in the flight arena, we constructed the UWB TDOA localization system with eight UWB anchors in centralized TDOA mode. The anchor positions were selected manually to cover the entire staircase space while maintaining line-of-sight between each other. In the ESKF algorithm, we increased the variance of UWB measurement noise to $\sigma_{ij}^2 = 0.015$ to address the corrupted UWB measurements encountered in this staircase scenario. We use a Leica total station in the tracking mode, which tracks the prism on the UWB handheld device and provides the position measurement at 5 Hz for ground truth.

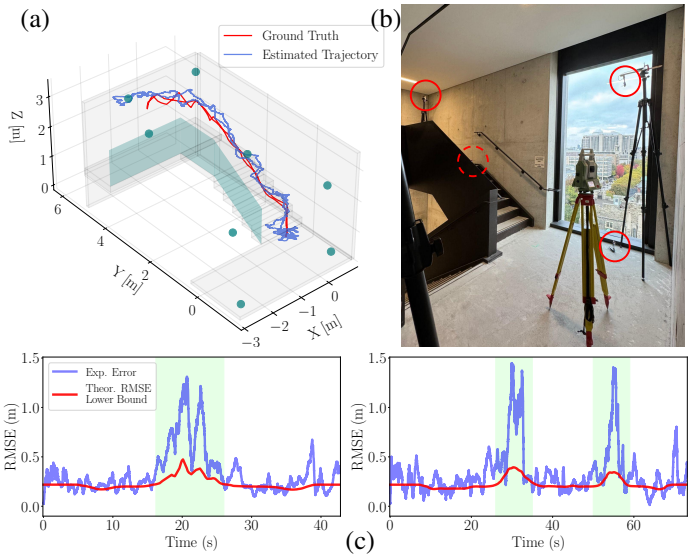

Fig. 7. The staircase scenario and our experimental setup are shown in (a) and (b). The experimental trajectory #1 and the corresponding ground truth trajectory are shown in (a). The ESKF estimation errors and the theoretical RMSE lower bounds along the trajectories are shown in (c).

To quantify the localization accuracy, we manually moved the handheld device at low speed to prevent the total station from losing track and conducted two experiments walking along the staircase. We demonstrate the ground truth trajectory of the first experiment along with the estimation results in Figure 7a. During the experiments, we moved the handheld device up-

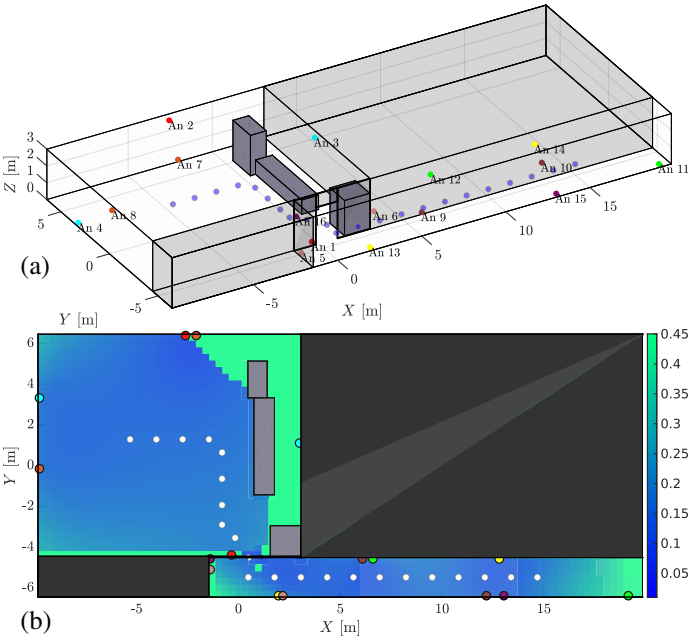

Fig. 8. The 3D layout of the multi-room environment, including a cafeteria and a narrow hallway, is shown in (a). The 22 sampled points representing the pre-defined trajectory are shown as blue dots in (a) and white dots in (b). The 16 UWB anchors in decentralized TDOA mode are designed through sensor placement optimization. The localization performance among the multi-room space is demonstrated in the heatmap (b), with lower RMSE indicated with darker color.

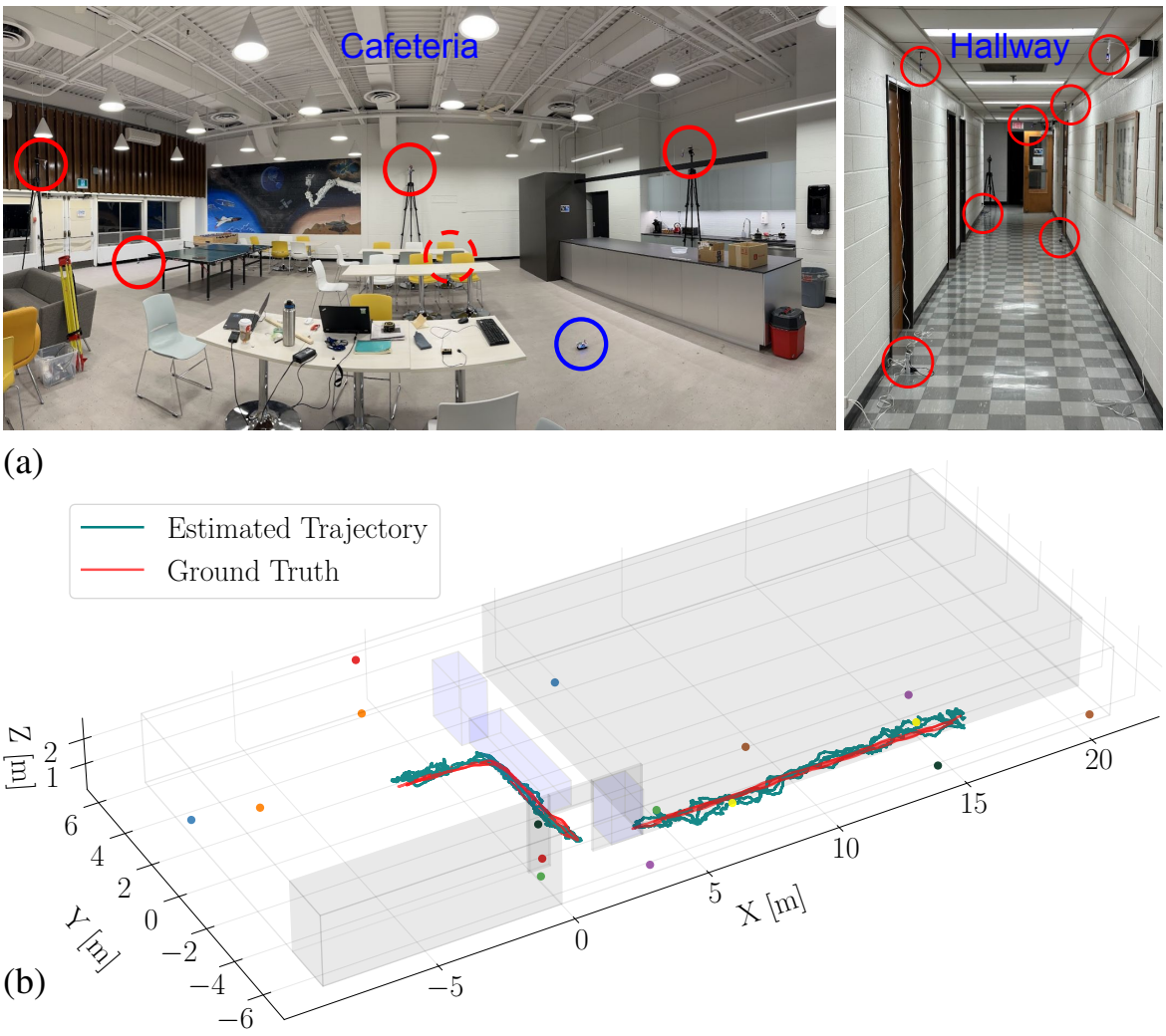

Fig. 9. Real-world deployment of the UWB TDOA localization system in the multi-room environment (a) based on the optimal sensor placement design. The anchors are enclosed by red circles and the UWB handheld device is highlighted with a blue circle. The estimated results together with the total station ground truth trajectories from all five experiments are summarized in (b). The experimental results show that the propose localization system achieves an average 28 centimeters positioning accuracy in this multi-room scenario.

stairs to the second floor and approached the boundary of the anchor constellation, which resulted in challenging anchor-tag geometry [6].

We compute the theoretical lower bound of the localization RMSE along the experimental trajectories through sensor placement analysis and present them together with the ESKF estimation errors over time in the bottom row of Figure 7c. Although the real-world ESKF estimation errors are considerably higher than the theoretical lower bound due to the challenging radio propagation conditions in the staircase, the theoretical values predicted the localization error peaks by analyzing the anchor-tag geometry. The localization performance degrades significantly around 20 seconds in trajectory #1 and around 30 and 55 seconds in trajectory #2, which correspond to the time that we approached the boundary of the anchor constellation. With the assistance of sensor placement analysis, we can evaluate the localization performance for regions or trajectories of interest and effectively predict any degradation in positioning accuracy. This information can be valuable for path planning algorithms of mobile robots, for example.

D. A Case Study: Localization in a Multi-room Scenario

To demonstrate the entire process of constructing a UWB TDOA localization system, we select a challenging multi-room scenario, which includes a cafeteria and a narrow hallway, as our case study. We selected the cafeteria and the hallway in the University of Toronto Institute for Aerospace Studies (UTIAS) as the experimental space. The multi-room space dimensions were obtained from the building blueprint with the height measured manually. The 3D layout of the multi-room environment, accurately scaled to reflect the real-world dimensions, is visualized in Figure 8a. We modeled the fridge, counter table, and the vending machine as metal obstacles that will lead to severe NLOS scenarios [6] and ignored the movable tables, chairs, and sofas in the cafeteria. As an illustrative example, we aimed to develop a UWB TDOA localization system with the goal of achieving a theoretical localization RMSE lower bound of 20 centimeters along a pre-defined trajectory from the center of the cafeteria to the end of the hallway. The desired RMSE lower bound value

only serves as one example of this case study and can be varied according to different design purposes. We configured the UWB anchors from Bitcraze into decentralized mode [20], which enables scalability in the number of anchors, to cover the entire space. The anchor positions were constrained to be on the boundary of the 3D space for installation purposes.

It is crucial yet challenging to find an optimal anchor placement to ensure reliable localization performance in such complicated environments. Consequently, we employed the optimal sensor placement algorithm [6] briefly introduced in Section III-B to optimize both the required number of anchors and their corresponding positions to meet the accuracy requirement. We selected 22 sample points to represent the predefined trajectory and optimize the anchor positions for them. In the sensor placement algorithm, we assume the UWB LOS measurements are unbiased with the default 10 centimeters standard deviation and ignore multi-path effects. The optimization results indicated that 16 anchors, arranged into 8 anchor pairs $\Gamma = \{(1,2),(3,4),\cdots,(15,16)\}$, are required to achieve an average RMSE lower bound of 20 centimeters over the sample points. The optimized anchor positions and the corresponding localization accuracy heatmap, with lower RMSE indicated with darker color, are visualized in Figure 8b. With the optimized anchor placement, each sampled point maintains LOS to several anchor pairs in this challenging environment to ensure reliable localization. As Bitcraze's UWB anchors communicate and synchronize among all nearby anchors in decentralized mode, UWB tag will receive out-of-sequence TDOA measurements $d_{ij} \notin \Gamma$. Since the out-of-sequence UWB measurements often suffer from degraded anchor geometries, we inflated the variance for $d_{ij} \notin \Gamma$ as 0.025 in the ESKF algorithm to fuse these measurements. We also increased the Mahalanobis distance parameter of the chi-squared test to 10 for outlier rejection to avoid rejecting too many measurements in this challenging environment.

After determining the number of anchors and their positions, we deployed the 16 UWB anchors in the UTIAS cafeteria and hallway according to the sensor placement design. The deployment of the localization system during the experiments is shown in Figure 9a. As explained in Section III-D, we constructed the inertial frame and surveyed the anchor positions within this frame using a Leica total station. The average RMSE between the deployed anchor positions compared to the designed positions is 22 centimeters, which is partially due to the inconsistency between the actual construction results and the building blueprints. However, this discrepancy is negligible compared to the overall scale of the space, which spans over 25 meters.

We follow the same procedure as the staircase experiments in Section IV-C and used the Leica total station to provide ground truth. However, due to the challenging geometry at the tight corners around the doorway, the total station lost track at the intersection of the cafeteria and the hallway. Consequently, we had to conduct experiments in the cafeteria and the hallway separately to obtain reliable ground truth position measurements to quantify the localization accuracy.

We conducted three experiments in the cafeteria and two experiments in the hallway following a predefined trajectory.

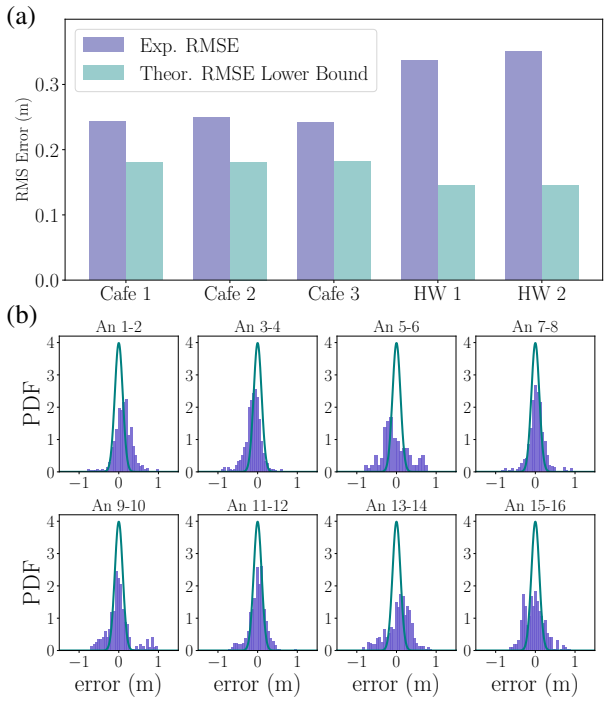

Fig. 10. Simulation and experimental root-mean-squared error (RMSE) results (a) and histograms of UWB TDOA measurement residuals in the multi-room environment (b). The default zero-mean Gaussian noise distribution $n_{ij} \sim \mathcal{N}(0, 0.01)$ under LOS conditions (green) is overlaid onto the histograms (blue) for comparisons. The UWB measurements are corrupted during the experiments, leading to the gap between the theoretical analysis and experimental results.

We summarize all the experimental results and demonstrate the estimated trajectories together with the total station ground truth trajectories in Figure 9b. The corresponding RMSE for each experiment and the theoretical RMSE analysis are summarized in Figure 10a. The average localization RMSE in the cafeteria and the narrow hallway are 24 centimeters and 34 centimeters, respectively, leading to an overall average of 28 centimeters in this multi-room environment.

Although the localization accuracies, considering the low-cost IMU and UWB sensors we used in this challenging environment, are commendable and sufficient for pedestrian localization applications, there remains a gap between theoretical analysis and experimental results. The average theoretical localization lower bound derived from sensor placement analysis is 17 centimeters. This gap is mainly caused by the differences in the UWB sensor noise model between theoretical analysis and real-world experiments. We present the UWB TDOA measurement error histograms among the five experimental trajectories in Figure 10b. The default zero-mean Gaussian noise distribution $n_{ij} \sim \mathcal{N}(0, 0.01)$ under LOS conditions is overlaid onto the histograms for comparison. It can be observed that the UWB measurements were severely corrupted compared to the default zero-mean Gaussian error distribution we used in the simulation, which leads to the gap between the real estimated RMSE and the theoretical analysis. In the sensor placement analysis, we assume that the UWB measurements are unbiased under LOS scenarios and neglect multi-path signal propagation. However, the radio propagation

environment was more challenging than the simulation setting, with UWB TDOA measurements corrupted by the intrinsic biases of the low-cost DW1000 UWB module [9] and multi-path propagation, especially in the narrow hallway.

To address this issue, we recommend a conservative sensor placement design by setting a higher standard deviation for LOS measurements within the algorithm. Alternatively, if there exists a method to better simulate and detect multi-path radio propagation in UWB communication, we can incorporate that into the sensor placement optimization to enhance the overall performance of the UWB TDOA localization system.

V. Conclusion

In this article, we presented a UWB TDOA localization system approached from a system-level perspective. We detailed a fully integrated system, from sensor placement optimization, hardware and software architecture, to real-world deployment and system evaluation. Our system provides accurate and robust localization service while maintaining a cost-effective, lightweight, and portable design. We conducted extensive experiments across various real-world environments, demonstrating its accuracy and robustness in multi-agent pedestrian localization, resilience to sensor occlusion, and the ability to evaluate the performance degradation using sensor placement analysis in a challenging staircase. Furthermore, we selected a multi-room environment, including a cafeteria and a narrow hallway, as a case study to exemplify the deployment of our entire UWB TDOA localization system. We started with sensor placement optimization for a pre-defined trajectory, proceeded to the system deployment, and concluded with an evaluation of the real-world localization performance against theoretical analysis. The experimental results show that the proposed UWB TDOA localization system can achieve around 28 centimeters positioning accuracy in this challenging multi-room environment spanning over 25 meters, which sheds light on radio-based, scalable, cost-effective, and lightweight indoor localization solutions.

VI. Acknowledgement

We would like to thank Adam Heins, Connor Jong, Keenan Burnett, and Sepehr Samavi for their assistance in the experiments. This work was supported in part by the Natural Sciences and Engineering Research Council of Canada (NSERC) and in part by the Canada CIFAR AI Chairs Program.

References

[1] S. E. Trevlakis, A.-A. A. Boulogeorgos, D. Pliatsios, J. Querol, K. Ntontin, P. Sarigiannidis, S. Chatzinotas, and M. Di Renzo, "Localization as a key enabler of 6G wireless systems: A comprehensive survey and an outlook," *IEEE Open Journal of the Communications Society*, vol. 4, pp. 2733–2801, 2023.

[2] K. Somasundaram, J. Dong, H. Tang, J. Straub, M. Yan, M. Goesele, J. J. Engel, R. De Nardi, and R. Newcombe, "Project Aria: A new tool for egocentric multi-modal AI research," *arXiv preprint arXiv:2308.13561*, 2023.

[3] Apple. (2022) Nearby interaction with UWB. [Online]. Available: https://developer.apple.com/nearby-interaction/

[4] P. K. Enge, "The global positioning system: Signals, measurements, and performance," *International Journal of Wireless Information Networks*, vol. 1, no. 2, pp. 83–105, 1994.

[5] W. Meng, L. Xie, and W. Xiao, "Optimal TDOA sensor-pair placement with uncertainty in source location," *IEEE Transactions on Vehicular Technology*, vol. 65, no. 11, pp. 9260–9271, 2016.

[6] W. Zhao, A. Goudar, and A. P. Schoellig, "Finding the right place: Sensor placement for UWB time difference of arrival localization in cluttered indoor environments," *IEEE Robotics and Automation Letters*, vol. 7, no. 3, pp. 6075–6082, 2022.

[7] Z. Zhang, "Parameter estimation techniques: A tutorial with application to conic fitting," *Image and vision Computing*, vol. 15, no. 1, pp. 59–76, 1997.

[8] J. Cano, G. Pagès, E. Chaumette, and J. LeNy, "Clock and power-induced bias correction for uwb time-of-flight measurements," *IEEE Robotics and Automation Letters*, vol. 7, no. 2, pp. 2431–2438, 2022.

[9] W. Zhao, J. Panerati, and A. P. Schoellig, "Learning-based bias correction for time difference of arrival ultra-wideband localization of resource-constrained mobile robots," *IEEE Robotics and Automation Letters*, vol. 6, no. 2, pp. 3639–3646, 2021.

[10] A. H. Nguyen, M. Rath, E. Leitinger, K. V. Nguyen, and K. Witrisal, "Gaussian process modeling of specular multipath components," *Applied Sciences*, vol. 10, no. 15, p. 5216, 2020.

[11] W. Zhao, A. Goudar, M. Tang, X. Qiao, and A. P. Schoellig, "Uncertainty-aware gaussian mixture model for UWB time difference of arrival localization in cluttered environments," in *IEEE/RSJ International Conference on Intelligent Robots and Systems (IROS)*. IEEE, 2023, pp. 5266–5273.

[12] K. Li, Z. Cao, and U. D. Hanebeck, "Continuous-time ultra-wideband-inertial fusion," *IEEE Robotics and Automation Letters*, vol. 8, no. 7, pp. 4338–4345, 2023.

[13] A. Goudar, T. D. Barfoot, and A. P. Schoellig, "Continuous-time range-only pose estimation," in *20th Conference on Robots and Vision (CRV)*. IEEE, 2023, pp. 29–36.

[14] I. Sharp, K. Yu, and Y. J. Guo, "GDOP analysis for positioning system design," *IEEE Transactions on Vehicular Technology*, vol. 58, no. 7, pp. 3371–3382, 2009.

[15] C. R. Rao, "Information and the accuracy attainable in the estimation of statistical parameters," in *Breakthroughs in Statistics: Foundations and basic theory*. Springer, 1992, pp. 235–247.

[16] S. Roumeliotis, G. Sukhatme, and G. Bekey, "Circumventing dynamic modeling: evaluation of the error-state Kalman filter applied to mobile robot localization," in *1999 IEEE International Conference on Robotics and Automation (ICRA)*, 1999, pp. 1656–1663 vol.2.

[17] Y. C. Eldar *et al.*, "Rethinking biased estimation: Improving maximum likelihood and the Cramér–Rao bound," *Foundations and Trends® in Signal Processing*, vol. 1, no. 4, pp. 305–449, 2008.

[18] A. Goudar and A. P. Schoellig, "Online spatio-temporal calibration of tightly-coupled ultrawideband-aided inertial localization," in *2021 IEEE/RSJ International Conference on Intelligent Robots and Systems (IROS)*. IEEE, 2021, pp. 1161–1168.

[19] J. Sola, "Quaternion kinematics for the error-state Kalman filter," *arXiv preprint arXiv:1711.02508*, 2017.

[20] W. Zhao, A. Goudar, X. Qiao, and A. P. Schoellig, "UTIL: An ultra-wideband time-difference-of-arrival indoor localization dataset," *The International Journal of Robotics Research*, vol. 0, no. 0, 2024, DOI: 10.1177/02783649241230640.